Spatial and Temporal Registration of CT and SPECT Images: Development and Validation of a Technique for In Vivo Three-Dimensional Semiquantitative Analysis of Bone

Mark P. Bernstein, Curtis B. Caldwell, Oleh M. Antonyshyn, Perry W. Cooper, and Lisa E. Ehrlich

Division of Plastic Surgery and Department of Medical Imaging, Sunnybrook and Women's College Health Sciences Centre, University of Toronto, Toronto, Ontario, Canada

The combined use of postoperative 3-dimensional CT and SPECT imaging provides a means of relating anatomy and physiology for the semiquantitative in vivo analysis of bone. This study focuses on the development and validation of a technique that accomplishes this through the registration of SPECT data to a 3-dimensional volume of interest (VOI) interactively defined on CT images. **Methods:** Five human cadaver heads served as anthropomorphic models for all experiments. Four cranial defects were created in each specimen with inlay and onlay split-skull bone grafts reconstructed to skull and malar recipient sites. To acquire all images, each specimen was landmarked with 1.6-mm ball bearings and CT scanned. Bone surfaces were coated with ^{99m}Tc-doped paint. The locations of the ball bearings were marked with paint doped with ^{111}In. Separate SPECT scans were acquired using the energy windows of ^{99m}Tc and ^{111}In. **Results:** Serial SPECT images aligned with an average root-mean-square (RMS) error of 3.8 mm (i.e., <1 pixel). CT-to-SPECT volume matching aligned with an RMS error of 7.8 mm. Total counts in CT-defined VOIs applied to SPECT data showed a strong linear correlation (r^2 = 0.86) with true counts obtained from a dose calibrator. **Conclusion:** The capability of this multimodality registration technique to anatomically localize and quantify radiotracer uptake is sufficiently accurate to warrant further assessment in an in vivo trial.

Key Words: SPECT; 3-dimensional CT; image registration; bone

J Nucl Med 2000; 41:1075–1081

Functional imaging of the craniofacial skeleton provides an important adjunct to the surgical management of craniofacial deformities. Precise preoperative delineation of areas of abnormal bone turnover guides the extent of resection required in the management of osteomyelitis or bone tumors. Serial postoperative imaging permits outcome evaluation of bone transplant procedures in terms of revascularization, osteoblastic activity, and, hence, viability.

Received Feb. 15, 1999; revision accepted Sep. 23, 1999.

For correspondence or reprints contact: Oleh M. Antonyshyn, MD, Division of Plastic Surgery, Rm. M1-525, Sunnybrook and Women's College Health Sciences Centre, 2075 Bayview Ave., Toronto, Ontario, M4N 3M5 Canada.

However, the routine application of functional imaging in the assessment of craniofacial skeletal deformities is limited. The relatively low resolution of nuclear medicine images and the difficulty of proper localization within the facial skeleton represent major restrictions. Bone scintigraphy using ^{99m}Tc-methylene diphosphonate (MDP) offers a means of in vivo physiologic monitoring of local bone metabolism. Radiopharmaceutical is adsorbed to hydroxyapatite crystals in bone proportional to osteoblastic activity and regional blood flow (*1*). Unfortunately, planar bone scans yield poor discrimination of overlapping structures, making accurate interpretation problematic. The evolution to SPECT provides 3-dimensional visualization of bone scans with enhancement of the signal-to-noise ratio (*1*). Clinically, bone scintigraphy alone has been used in the postoperative monitoring of vascularized bone transfers (*2–4*) and in establishing graft viability in long-term follow-up of free bone grafts (*5,6*). Despite this advancement, SPECT images lack sufficient anatomic resolution, which limits those clinical applications in which precise localization or quantitative information is important. This limitation has been recognized previously, and multimodality image registration offers a potential solution.

Three-dimensional multimodality image registration techniques enable the fusion of 2 images from different modalities, or from different times, for further analysis. Structural images (CT) may be matched with functional images (SPECT) to improve the interpretation of the relatively low-resolution nuclear medicine scans. Similarly, serial registrations of images from the same imaging modality, in the same patient, permit direct comparison and interpretation of temporal anatomic or physiologic changes (or both).

Multimodality image registration has in fact been used in mapping structure to function in brain CT, MRI, and PET data (*7*); the evaluation of chronic osteomyelitis (*8,9*); and the determination of sequestrum activity (*10*). Although these previous efforts have focused primarily on fusing and displaying 2 images together, the alignment of structural (CT) and functional (SPECT) images is only the first step. Our methodology offers a further refinement. Once a region

of interest (ROI) on CT is defined, a 3-dimensional volume of interest (VOI) is generated and subsequently registered to a ^{99m}Tc-MDP SPECT scan. Once fused, the ^{99m}Tc uptake per unit volume can be quantified in an anatomically correct object. Moreover, serial registrations permit in vivo monitoring of the ^{99m}Tc uptake to accurately assess long-term bone viability.

The objectives of this research study were to develop a technique for spatial and temporal registration of CT and SPECT images and to validate the technique—specifically, to determine the accuracy of serial 3-dimensional SPECT and SPECT–CT image alignment and the accuracy of CT-guided semiquantitative SPECT uptake measurements.

MATERIALS AND METHODS

Surgical Protocol

Five preserved cadaver heads were obtained from the University of Toronto anatomy department. Soft tissues, including periosteum, were partially dissected off the skull. Craniotomies of approximately 40 × 30 mm were performed bilaterally in the frontoparietal and posterior parietal skull, resulting in 4 full-thickness skull defects and 4 bicortical cranial bone grafts. The harvested grafts were split through the diploe into inner and outer tables, simulating the clinical scenario (Figures 1 and 2). Inner table grafts were returned to their respective donor sites as inlay grafts, whereas outer table grafts were placed on the malar regions of the corresponding skull as onlay grafts. Grafts were secured and rigidly fixed with Leibinger 1.2-mm titanium microplates and screws (Howmedica Leibinger, Inc., Dallas, TX). Rigid stabilization simulates the clinical situation and eliminates error from graft movement during and between image acquisitions.

CT Imaging Protocol

Holes (1.6-mm diameter) were drilled to a depth of 0.8 mm in 8 locations on each skull. Ball bearings (1.6-mm diameter) were inserted in each hole to provide CT contrast. CT scans were acquired with a HiSpeed Advantage scanner (General Electric Medical Systems, Milwaukee, WI). Axial slices (3-mm thick) were obtained from the vertex to the mentum. The field of view was set to 24 cm with 120 kVp, 400 mAs. Images were reconstructed as 512 × 512 pixel arrays and window levels were set to show bony structures (window = 2000, level = 300).

Segmentation of VOIs

The CT data were transferred to an Allegro computer workstation (ISG Technologies, Toronto, Canada) for 3-dimensional reconstruction and manipulation. After selection of appropriate thresholding parameters, the individual inlay and onlay grafts were interactively identified and traced on serial axial slices. The segmented pixels in consecutive axial slices were then reconstructed to form 3-dimensional objects representing the cranial bone grafts or VOIs (Fig. 3).

SPECT Imaging Protocol

All exposed skull surfaces were painted with a solution containing ^{99m}Tc. Because complete dissection of all soft tissue from the surface of a skull is a difficult and tedious task, complete dissections were not attempted, particularly to levels well below those used for inlay grafts. Thus, not all bone surfaces could be painted. The skulls were allowed to dry for 1 h. The 8 ball-bearing locations were then marked with ^{111}In-doped paint. The skulls were allowed to dry for an additional hour. Two sequential SPECT acquisitions were then made for each skull using a triple-head γ camera fitted with high-resolution, parallel-hole collimators (Picker 3000; Picker International, Cleveland, OH). The first acquisition was intended to capture an image of the ^{99m}Tc distribution (TC-SPECT1). The energy window was therefore set at 140 keV with a 15% width. One hundred twenty frames were acquired, in step-and-shoot mode, with each frame acquired for 25 s. Each frame was 128 × 128 pixels in size. Without moving the skull, a second acquisition was made to capture the image of the ^{111}In markers (IN-SPECT1). Two energy windows were used: centered at 173 keV (20% energy window) and 246 keV (20% energy window). The ^{111}In acquisition was identical to the ^{99m}Tc acquisition except for the energy window and the time per frame, which was increased to 40 s. The radius of rotation was 13.5 cm for all acquisitions. Transaxial images (128 × 128 pixels) were reconstructed over a 300-mm field of view from each acquisition using standard filtered backprojection techniques. After reconstruction, the images were corrected for photon attenuation using the first-order Chang method (*11*). The reconstructed slice thickness was 3.56 mm. Pixels were square in the transaxial plane and measured 2.34 × 2.34 mm. Examples of ^{99m}Tc and ^{111}In SPECT images are shown in Figure 4. This camera had a measured spatial resolution of ~10 mm full width at half maximum (FWHM) for ^{99m}Tc SPECT.

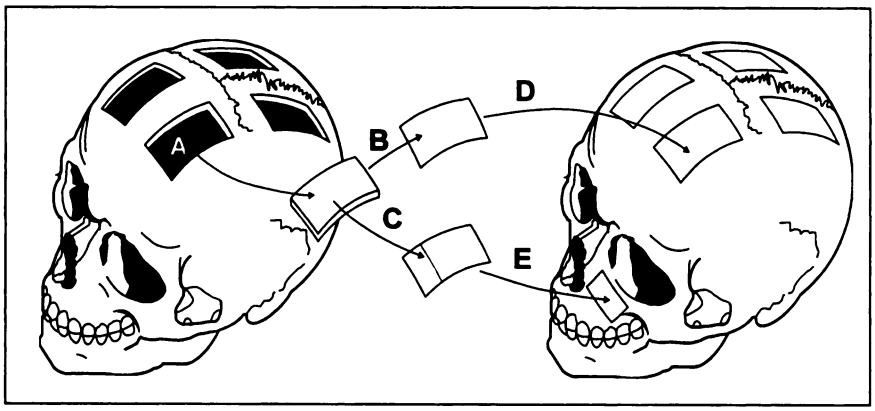

FIGURE 1. Cadaver surgery protocol. Four craniotomies are performed in each skull. Procedure is illustrated for left frontoparietal site only. (A) Craniotomy provides full-thickness (bicortical) cranial bone graft. Cranial bone graft is then split through diploe, providing inner table (B) and outer table (C) cortical grafts. (D) Inner table bone segment is applied as inlay graft to reconstruct craniotomy site. (E) Outer table segment from 2 grafts per skull is applied as onlay graft to malar region.

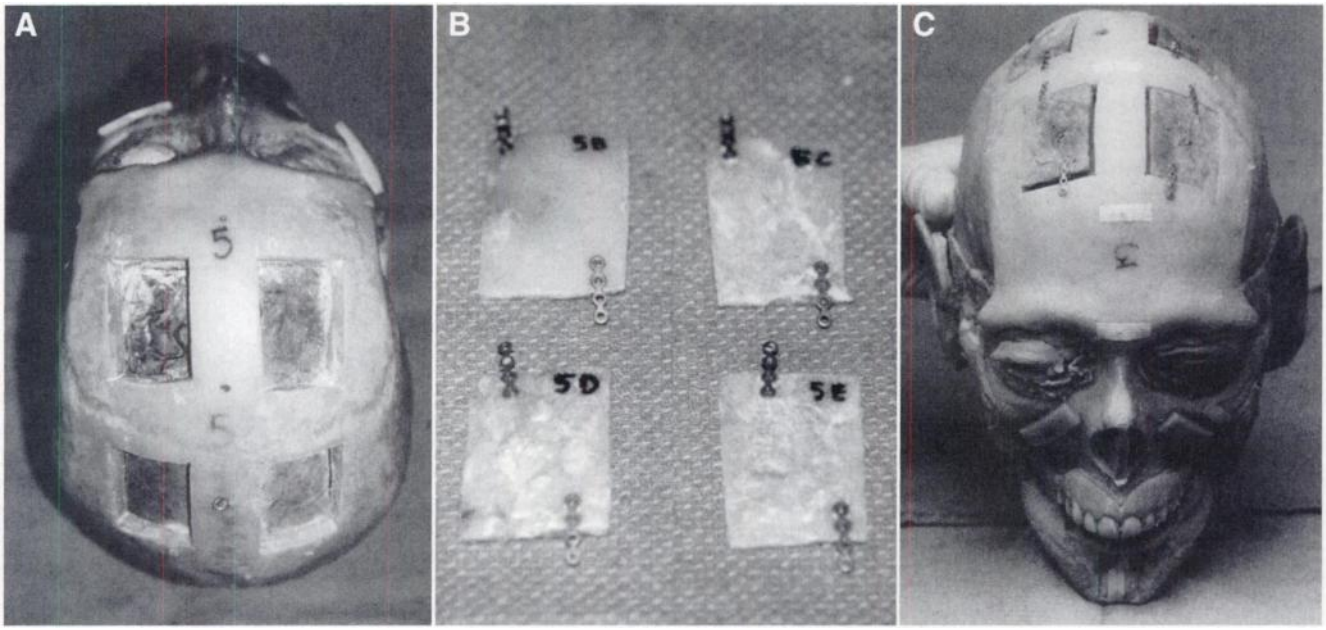

FIGURE 2. (A) Vertex view of cadaver head 5, subsequent to craniotomy but before placement of inlay grafts. (B) Labeled inlay grafts for head 5. (C) Anterior view of head 3, illustrating placement of 4 inlay and 2 onlay grafts.

SPECT–CT Registration

^{99m}Tc SPECT scans were aligned with CT scans using an automated, volume-matching algorithm originally developed for aligning PET images with MR images of the brain (*12*). In this algorithm, the CT image is partitioned into 256 separate components on the basis of CT voxel values. An iterative technique that searches among a range of transformations is then applied to minimize the weighted average of the SDs of SPECT voxel values corresponding to the different CT components. The principle behind this technique is that similar CT tissue types should also have similar SPECT uptake values. We applied this technique because of our familiarity with it for SPECT–nuclear magnetic resonance (NMR) brain image matching. Neither the ball bearings nor the ^{111}In markers were used in the alignment phase. The algorithm uses a rigid body rotation and translation model involving 3 rotational and 3 translational degrees of freedom. Thus, once alignment of image A with image B has been performed, a transformation matrix is produced, which represents the rotations and translations that are required. If an additional image, C, exists that was originally aligned with image A, then the same transforma-

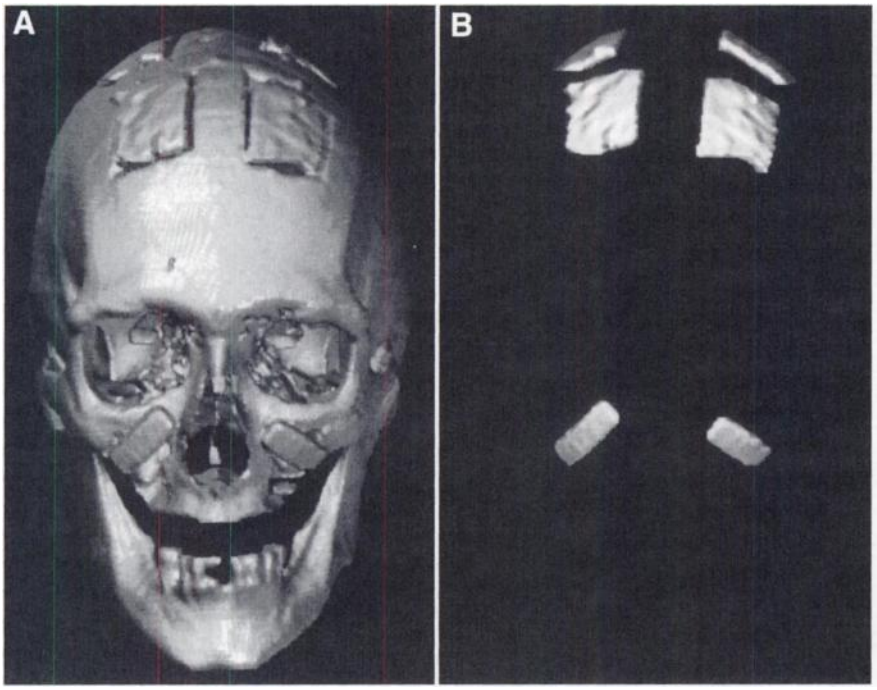

FIGURE 3. (A) Anterior view of 3-dimensional surface reconstruction of CT data from head 3. (B) Segmented CT VOIs for 4 inlay and 2 onlay grafts of head 3.

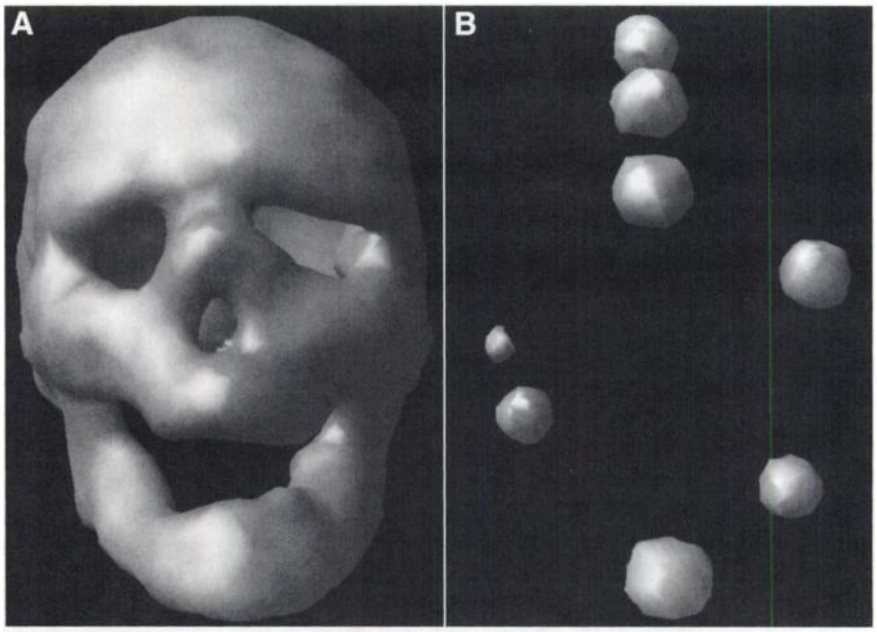

FIGURE 4. Anterior views of 3-dimensional surface reconstructions of ^{99m}Tc SPECT scan of specimen 5 (i.e., painted surfaces of specimen) (A) and ^{111}In SPECT scan of specimen 5 (i.e., ^{111}In markers) (B).

tion matrix can be used to align image C with image B. Once the ^{99m}Tc image was aligned with the CT scan, the same rigid body transformation was applied to the ^{111}In SPECT image.

The error in SPECT–CT alignment was assessed by measuring the distance between the center of the ^{111}In markers in the aligned ^{111}In image and the center of the ball bearings in the CT image. The 3-dimensional location of the center of each ^{111}In marker was found using a center-of-mass calculation. In this method, transaxial slices from the ^{111}In dataset were first displayed. An observer placed a cursor in the area of the marker in question. A computer program then extracted a 2 × 2 × 2 cm block of pixels surrounding the selected pixel. The x coordinate of the center of activity was calculated from the equation: $x_{ca} = (\Sigma a_i x_i)/(\Sigma a_i)$, where a_i is the number of counts recorded in pixel i. The y and z centers of activity are found in similar fashion. This center-of-activity method allowed us to calculate the location of the center of the ^{111}In marker to subpixel accuracy. Because of the comparatively high resolution of the CT scans, the x, y, and z location of the center of the ball-bearing markers was found manually by placing a cursor in the center of each marker in images that had been "zoomed" by a factor of 2.

SPECT–SPECT Registration

Three days after the original SPECT acquisitions (to allow the original ^{99m}Tc to decay), the skulls were again painted with ^{99m}Tc, and both SPECT scans were again obtained (i.e., TC-SPECT2 and IN-SPECT2). Because of the 2.8-d half-life of ^{111}In, it was unnecessary to repaint the marker sites. TC-SPECT2 was aligned with TC-SPECT1 using the automated technique (*11*). The transformation matrix thus derived was applied to the IN-SPECT2 scan. Individual ^{111}In marker positions were defined by applying a center-of-mass calculation to a 3-dimensional subregion surrounding the marker in the ^{111}In image as in the SPECT–CT alignment task. The difference in position of the ^{111}In markers in IN-SPECT1 and in the aligned version of IN-SPECT2 provided an estimate of alignment error (Figs. 5A and B).

CT-Guided SPECT Uptake

Analysis of CT-guided SPECT uptake measurements was performed by coating the skull and grafts with different, known amounts of ^{99m}Tc-doped paint. The total activity on each graft was measured using a radionuclide dose calibrator (CRC-12 radioisotope calibrator; Capintec Instruments, Inc., Ramsey, NJ) before rigid fixation. A third set of ^{99m}Tc SPECT images was obtained for each specimen (i.e., TC-SPECT3). These images were aligned with the version of TC-SPECT1 that had been aligned previously with CT scan images. Direct alignment of the TC-SPECT3 images with the CT images was not possible because of the highly nonuniform radionuclide distribution used in TC-SPECT3. The alignment algorithm used works best when all bone has similar SPECT intensity. (Although all bone-exposed bone surfaces were coated with radioactive paint for all SPECT acquisitions, the distribution of activity in TC-SPECT3 was highly inhomogeneous because of the desire to have a large range of activities on the various graft sites.) VOIs representing the inlay grafts in the CT images were defined as described. These VOIs were applied to the aligned TC-SPECT3 data. A correction for the decay of ^{99m}Tc was applied to all activity data. We thus obtained total counts in each VOI region for all inlay grafts. These values were compared with the activity values obtained from the dose calibrator measurements (Fig. 5C).

RESULTS

SPECT–SPECT Alignment

After alignment of TC-SPECT2 (and IN-SPECT2) with TC-SPECT1, marker positions in the 2 corresponding ^{111}In images were compared. The accuracy of alignment of serial SPECT images was determined by comparing the marker positions in the 2 ^{111}In images and assessing the root-mean-square (RMS) error. The RMS error ranged from 0.42 to 8.62 mm, with a mean RMS error of 3.8 mm for all markers (Table 1; Fig. 6). In 2 cases, markers could not be evaluated (both at position 8, but for heads 2 and 4). In both cases, an ^{111}In marker could not be visualized properly at position 8, probably because of inadequate marking of the point with ^{111}In-doped paint.

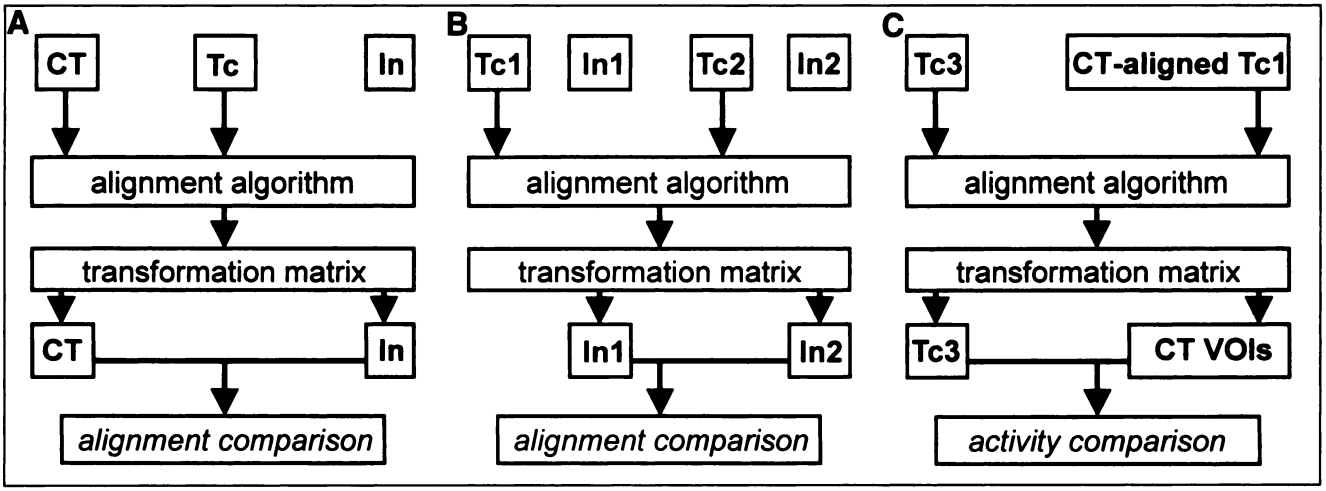

FIGURE 5. (A) SPECT–CT alignment. ^{99m}Tc SPECT scan is acquired and aligned with CT scan and resulting transformation matrix is applied to ^{111}In SPECT scan. Positions of ^{111}In markers are compared with CT ball bearings. (B) Serial SPECT registration. Two ^{99m}Tc SPECT acquisitions acquired 3 d apart (TC-SPECT1 [Tc1] and TC-SPECT2 [Tc2]) are aligned, and resulting transformation matrices are applied to 2 complementary ^{111}In SPECT scans 3 d apart (IN-SPECT1 [In1] and IN-SPECT2 [In2]). Alignment accuracy of ^{111}In markers is measured. (C) SPECT–CT uptake protocol. ^{99m}Tc SPECT3 (Tc3) scan is acquired and aligned with previously CT-aligned SPECT study (A). CT-defined VOIs are then aligned with TC-SPECT3 scan, and total counts are obtained and compared with dose calibrator measurements.

SPECT–CT Alignment

The accuracy of alignment of CT and SPECT images was determined by comparing CT ball-bearing positions with ^{111}In marker positions and assessing the RMS error. The RMS error ranged from 1.7 to 11.5 mm, with a mean RMS error of 7.8 mm for all markers (Table 2). One marker position could not be evaluated (marker 8, head 2) because the ^{111}In marker was not visualized properly in IN-SPECT1. Note that marker 8, located on the chin, was the marker farthest from the area of interest—i.e., the graft regions near the forehead and skull vertex. Visually, the most obvious errors appeared to consist of errors of rotation, as opposed to errors in which 1 dataset was mistranslated versus the other.

CT-Guided SPECT Uptake Measurement

VOIs defined on CT were applied to aligned TC-SPECT3 scans. Total counts in CT-defined VOIs were compared with activity measurements (kilobecquerels) obtained from the dose calibrator. The r^2 statistic for a linear regression was 0.86, with an SE of the regression of 330 counts (Fig. 7).

TABLE 1
Accuracy of SPECT–SPECT Alignment

Head no.	Marker							
	1	2	3	4	5	6	7	8
1	1.76	1.38	0.697	1.58	0.474	0.424	1.31	2.88
2	4.52	3.04	2.10	2.20	3.72	5.49	5.18	NE
3	7.15	5.69	4.36	3.37	5.96	1.58	7.06	5.63
4	5.83	8.62	7.49	2.87	6.96	7.81	5.77	NE
5	4.74	1.43	2.48	4.72	4.28	3.11	3.52	5.92

NE = not evaluated.

For each cadaver head, RMS distance (mm) between each marker on SPECT1 and aligned SPECT2 is tabulated. Overall average RMS alignment error = 3.8 mm.

DISCUSSION

Although multimodality image registration techniques have been used for aligning images of other areas of the body, they have been used most commonly to align images of the brain, relating structure to function (*7*). Recently, structural (CT and MRI) and functional (MRI, SPECT, and PET) images have been aligned for various clinical applications. Although bone scintigraphy alone has been used to monitor vascularized bone transfers (*2–4*) and viability of free bone grafts (*5,6*), the lack of anatomic precision has made patient diagnosis and management difficult. Consequently, Robinson and Higginbotham-Ford (*10*) reported the usefulness of combined scintigraphic and tomographic imaging in the evaluation of chronic osteomyelitis. They determined that multimodality image registration was complementary in localization of sequestrum and assessment of disease activity, aiding in successful medical and surgical treatment.

In this study, a technique developed for brain image registration was applied to the conceptually simpler task of aligning 3-dimensional multimodality images (CT and SPECT) of the skull. SPECT–SPECT bone scan alignment had a mean RMS error of 3.8 mm. This is a satisfactory result, considering the relatively poor resolution of the imaging technique (FWHM $\approx$ 10 mm). However, the mean RMS error for SPECT–CT alignment, 7.8 mm, is less satisfactory. One possible explanation is that there was an energy window spatial registration error that artificially exaggerated the misalignment—that is, if images acquired with the ^{111}In and ^{99m}Tc energy windows did not align, then the ^{111}In points would not align well with the ball bearings,

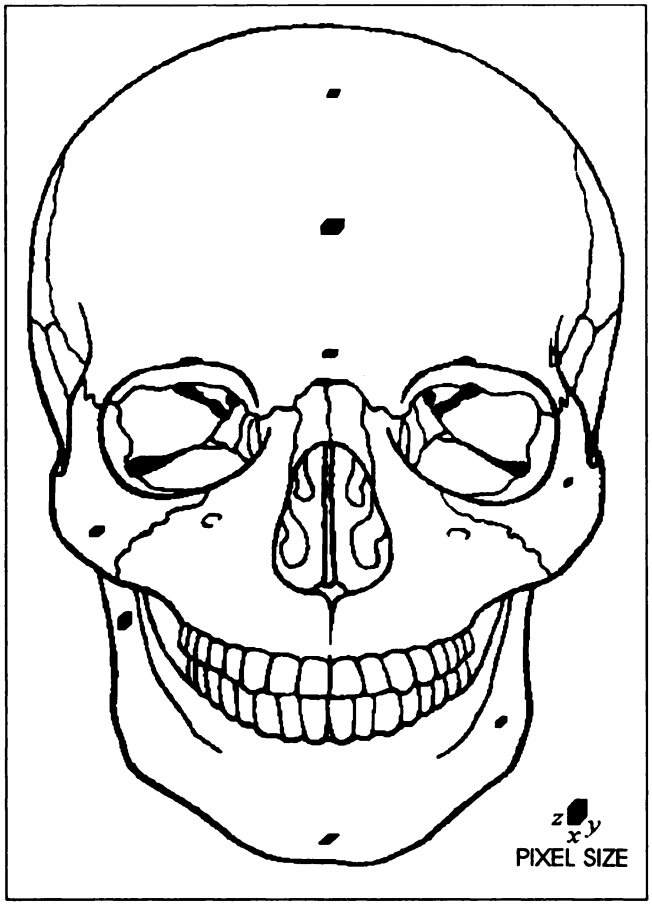

FIGURE 6. Average x, y, and z SPECT–SPECT alignment errors are shown as error boxes at each of 8 marker positions relative to skull and pixel size. Note that each position aligns within 1 pixel.

even if the ^{99m}Tc images aligned well with CT images. Although multiple-window spatial registration (MWSR) was not tested at the time of the experiment, it had been tested using the 3 energy windows of ^{67}Ga ~1 mo before the time of this experiment. At that time, the MWSR error was <0.5 mm, so it is unlikely that MWSR error was a major factor. Part of the alignment error may be explained by the

TABLE 2
Accuracy of SPECT–CT Alignment

Head no.	Marker 1	2	3	4	5	6	7	8
1	6.38	7.39	5.35	6.92	4.35	6.72	3.86	8.78
2	10.5	7.47	5.52	1.70	8.62	9.32	3.55	NE
3	9.75	9.42	8.64	6.75	8.59	5.29	11.48	11.46
4	9.09	9.76	9.36	9.90	9.40	8.68	9.74	14.2
5	9.47	6.01	3.44	3.48	5.78	8.62	9.17	12.4

NE = not evaluated.

For each cadaver head, RMS distance (mm) between each marker on CT1 and aligned SPECT2 is tabulated. Overall average RMS alignment error = 7.8 mm.

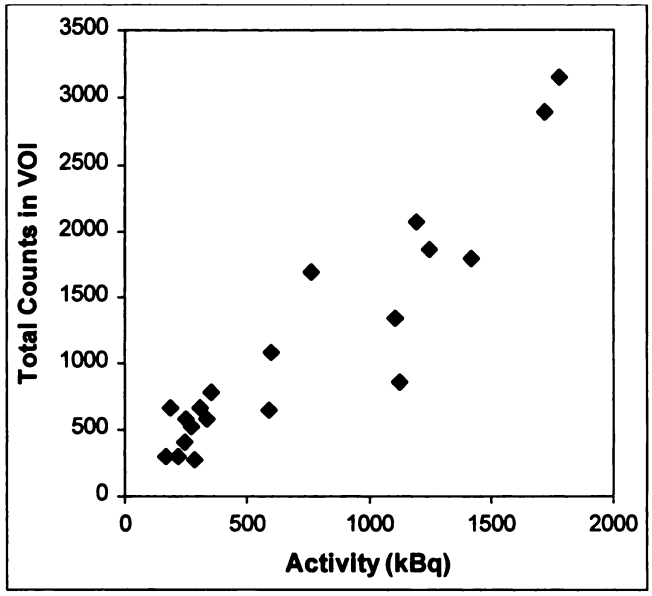

FIGURE 7. Total counts measured in TC-SPECT3 using VOIs defined on aligned CT scan versus graft activity as measured in dose calibrator. n = 20 (4 inlay grafts for each head were measured). r^2 for linear regression = 0.86.

experimental technique. We attempted to align SPECT images of painted exterior skull surfaces with CT images of whole cadaver heads. In addition, the technique we used was the volume-matching algorithm developed by Woods et al. (*12*). Although it might have been more appropriate to apply a surface-matching algorithm (*7*) and match the surface SPECT images with an exterior bone surface image extracted from the CT scans, in the clinical scenario the radiotracer uptake would indeed occur within the bone and not on the surface. Despite the SPECT–CT results, the VOIs defined on CT seem to be capturing the appropriate regions of the SPECT scan as shown by the plot of total counts measured in CT-guided VOIs versus dose calibrator–measured graft activity (Fig. 7), with a corresponding r^2 of 0.86 in the CT-guided SPECT uptake experiment. Perhaps this is a consequence of using the entire graft instead of a 1-mm marker for comparison. Essentially, the capability of this technique to localize and quantify uptake is promising.

Clearly, our existing technique is not completely accurate. Figure 7 shows some points that deviate significantly from the predicted level of activity. Several effects, including scatter, errors in attenuation correction, partial-volume effects, and SPECT–CT misalignment, may explain much of this variation. One should note that we did not apply a scatter correction to the SPECT images. In the normal clinical situation, relative, not absolute, uptake is most important. If one is evaluating the revascularization of a graft using sequential SPECT scans, the scatter conditions experienced at the location of the graft can reasonably be assumed to be similar at each time point. Therefore, it is not as essential to correct for such effects clinically as it may have been in this experiment. In addition, we do not routinely apply such corrections in clinical bone SPECT imaging. Scatter correc-

tions are also less likely to be more complex at tissue–air interfaces, which is essentially the situation near cranial bone grafts.

One reason for the relatively large scatter around the regression line in Figure 7 may be that the errors in both a SPECT–SPECT alignment and a SPECT–CT alignment were combined (because it was not possible to align TC-SPECT3 directly with a CT scan). In essence, we believe that the cadaver model described was a more difficult test than that of the clinical situation, in which the same area would be evaluated in SPECT scans taken at different time points. We have found SPECT–SPECT image alignment to be simpler and more accurate than SPECT–CT alignment. This would imply that, even if SPECT–CT alignment were imperfect, at least the same anatomic area would be evaluated on each sequential SPECT scan.

CONCLUSION

This technique provides a means of semiquantitative in vivo evaluation of vascular perfusion and osteoblastic activity in specific user-defined segments of bone. Potential clinical applications are varied. First, vascularized bone transfers are generally used in the reconstruction of unfavorable recipient sites; therefore, their success relies on maintenance of adequate vascular perfusion to the transferred bone. This technique allows direct determination of regional blood flow and of the degree of viability in transferred bone, compared with the donor site, and may prove to be a valuable adjunct in selecting optimal donor sites. Second, free bone grafts and bone substitutes undergo a process of resorption, revascularization, replacement, and eventual osseointegration. The ultimate outcome of various donor sources under varying recipient site conditions has not been determined previously because of the difficulty in evaluating bone graft survival in vivo. However, this technology permits precise delineation of the bone graft and direct monitoring of the rate and degree of revascularization until homeostasis is achieved. Third, osteomyelitis and certain bone tumors result in abnormal ^{99}Tc uptake. Precise anatomic delineation of these regions may prove to be valuable in planning and monitoring therapeutic interventions.

ACKNOWLEDGMENTS

The authors gratefully acknowledge the assistance of Karen Ma, research assistant; Pervaiz Kahn, imaging technologist; and the nuclear medicine and CT staff at Sunnybrook and Women's College Health Sciences Centre. This study was supported in part by a research grant from Howmedica Leibinger.

REFERENCES

1. Fig LM, Shulkin BL, Sullivan MJ, Rubinstein MI, Baker SR. Utility of emission tomography in evaluation of mandibular bone grafts. *Arch Otolaryngol Head Neck Surg*. 1990;116:191–196.
2. Takato T, Harii K, Nakatsuka T. The sequential evaluation of bone scintigraphy: an analysis of revascularized bone grafts. *Br J Plast Surg*. 1988;41:262–269.
3. Karcher H, Fuger G, Borbely L. Bone scintigraphy of vascularized bone transfer in maxillofacial surgery. *Oral Surg Oral Med Oral Pathol*.1988;65:519–522.
4. Bite U, Jackson IT, Wahner HW, Marsh RW. Vascularized skull bone grafts in craniofacial surgery. *Ann Plast Surg*. 1987;19:3–15.
5. Gordon SL, Binkert BL, Rashkoff ES, Britt AR, Esser PD, Stichfield FE. Assessment of bone grafts used for acetabular augmentation in total hip arthroplasty: a study using roentgenograms and bone scintigraphy. *Clin Orthop*. 1985;201:18–25.
6. Sanzen L, Fredin HO, Johnsson K, Nosslin B. Fate of bone grafts in acetabular roof reconstructions assessed by roentgenography and scintigraphy. *Clin Orthop*. 1988;231:103–109.
7. Pelizzari CA, Chen GTY, Spelbring DR, Weichselbaum RR, Chen CT. Accurate three-dimensional registration of CT, PET, and/or MR images of the brain. *J Comput Assist Tomogr*. 1989;13:20–26.
8. Weber PC, Seabold JE, Graham SM, Hoffmann HH, Simonson TM, Thompson BH. Evaluation of temporal and facial osteomyelitis by simultaneous In-WBC/Tc-99m-MDP bone SPECT scintigraphy and computed tomography scan. *Otolaryngol Head Neck Surg*. 1995;113:36–41.
9. Seabold JE, Simonson TM, Weber PC, et al. Cranial osteomyelitis: diagnosis and follow-up with In-111 white blood cell and Tc-99m methylene diphosphonate bone SPECT, CT, and MR imaging. *Radiology*. 1995;196:779–788.
10. Robinson CB, Higginbotham-Ford EA. Determination of sequestrum activity by SPECT with CT correlation in chronic osteomyelitis of the head and neck. *J Otolaryngol*. 1986;15:279–281.
11. Chang L-T. A method for attenuation correction in radionuclide computed tomography. *IEEE Trans Nucl Sci*. 1978;NS-25:638–643.
12. Woods RP, Mazziotta JC, Cherry SR. MRI-PET registration with automated algorithm. *J Comput Assist Tomogr*. 1993;17:536–546.